Resonances with triaxial deformation in the complex scaled Green's function method[*]

Xin-Xing Shi(史新星)[1]   Quan Liu(刘泉)[2]   Min Shi(仕敏)[3]   Zhong-Zhou Ren(任中洲)[1,4;1)]

[1] School of Physics, Nanjing University, Nanjing 210093, China
[2] School of Physics and Materials Science, Anhui University, Hefei 230601, China
[3] School of Mathematics and Physics, Anhui jianzhu University, Hefei 230601, China
[4] School of Physics Science and Engineering, Tongji University, Shanghai 200092, China

Abstract: We extend the complex scaled Green's function (CGF) method to describe resonances with triaxial deformation and present a theoretical formalism. Taking ^{43}S as an example, we elaborate numerical details and demonstrate how to determine the resonance parameters. With changes in the deformation parameters, we study the influence of the triaxial deformation parameter γ on single-particle levels. In particular, the present scheme focuses on the advantages of the complex scaling method (CSM) and the Green's function method, and is suitable for the exploration of resonances.

Keywords: resonances, single-particle levels, complex scaled Green's function (CGF) method

PACS: 25.70.Ef, 21.10.Pc, 27.40.+z   **DOI:** 10.1088/1674-1137/42/11/114105

1   Introduction

Over 85% of nuclei in the nuclear chart have deformed shapes [1]. The "deformed shapes" provide an intuitive understanding of the nuclear structure. Some nuclei have triaxial shapes [2], which can be characterized by the quadrupole triaxial deformation parameter γ besides the axial deformation parameter β. There are several islands of axial asymmetry on the nuclear chart, and most of them turn out to be triaxially deformed in their ground states [3]. This breaking phenomenon of axial symmetry is attracting more attention than before, with research in topics such as nuclear dynamical properties [4], the increase of the binding of nucleons [3], the loss of traditional magic numbers [5], shape coexistence [6], and so on. Although the triaxial nuclei cannot be measured directly, nuclear wobbling [7] and chiral bands [8, 9] have been used to infer the existence of triaxiality in the past decades. For exploring triaxiality, a series of models and methods have been established, including the five-dimensional collective Hamiltonian (5DCH) theory [10], the cranked Woods-Saxon (WS) shell model [11], the antisymmetrized molecular dynamics (AMD) combined with the generator coordinate method (GCM) [5], and so on.

In Ref. [12], we used the complex scaled Green's function (CGF) method to study ^{45}S under axial deformation, and the superiority of the method was shown. Furthermore, the resonance has resulted in the discovery of exotic phenomena of the deformed nuclei. This has triggered our interest in sulfur isotope research by probing the resonance states. ^{45}S and ^{43}S are neutron-rich nuclei, whose low-lying spectrum can provide the neutron single-particle levels. This can help us better understand the energy level structure to obtain the nuclear properties. Since deformed structures have had a profound effect on the development of nuclear physics, we apply the CGF method to the triaxially deformed nucleus ^{43}S [5], which is characterized by the quadrupole deformation parameters β and γ.

2   Formalism

To explore the resonances in a deformed system, the surface radius [7] can be expanded as

$$R(\theta,\varphi) = R_0\left\{1+\sum_{lm}\beta_{lm}Y_{lm}(\theta,\varphi)\right\}, \qquad (1)$$

when β_{lm} denotes the deformations deviating from the spherical shape and R_0 is the equilibrium radius. As the radius $R(\theta,\varphi)$ is real and $Y_{lm}^* = (-1)^m Y_{l,-m}$, we can obtain $\beta_{lm}^* = (-1)^m \beta_{l,-m}$. For simplicity, we introduce a set

of real parameters a_{lm} and b_{lm} to describe the deformations:

$$\begin{aligned}\beta_{l0} &= a_{l0},\\ \beta_{lm} &= \frac{a_{lm}-\mathrm{i}b_{lm}}{\sqrt{2}},\\ \beta_{l,-m} &= (-1)^m\frac{a_{lm}+\mathrm{i}b_{lm}}{\sqrt{2}},(m>0).\end{aligned} \quad (2)$$

By using the real parameters a_{lm} and b_{lm}, the surface is represented as

$$\begin{aligned}R(\theta,\varphi)&=R_0\Big\{1+\sum_{lm}\beta_{lm}Y_{lm}(\theta,\varphi)\Big\}\\ &=R_0\Big\{1+\sum_{l}a_{l0}Y_{l0}+\sum_{lm}\beta_{lm}Y_{lm}(\theta,\varphi)\\ &\quad+\sum_{l,-m}\beta_{l,-m}Y_{l,-m}(\theta,\varphi)\Big\},(m>0)\\ &=R_0\Big\{1+\sum_{l}a_{l0}Y_{l0}+\sum_{l,m>0}[\frac{a_{lm}-\mathrm{i}b_{lm}}{\sqrt{2}}Y_{lm}\\ &\quad+(-1)^m\frac{a_{lm}+\mathrm{i}b_{lm}}{\sqrt{2}}Y_{l,-m}]\Big\}.\end{aligned} \quad (3)$$

Then, we further express this as

$$R(\theta,\varphi)=R_0\left\{1+\sum_{l}a_{l0}Y_{lo}+\sum_{l,m>0}(a_{lm}Y_{lm}^++b_{lm}Y_{lm}^-)\right\}, \quad (4)$$

where $Y_{lm}^+=\frac{Y_{lm}+Y_{lm}^*}{\sqrt{2}},Y_{lm}^-=\frac{Y_{lm}-Y_{lm}^*}{i\sqrt{2}},Y_{lm}^*=(-1)^mY_{l,-m}$. For a quadrupole deformed system in the intrinsic framework, the Bohr description of deformation is

$$\begin{aligned}R(\theta,\varphi) &= R_0\{1+a_{20}Y_{20}+a_{22}(Y_{22}+Y_{2,-2})\},\\ a_{20} &= \beta_2\cos\gamma, \qquad a_{22}=\frac{1}{\sqrt{2}}\beta_2\sin\gamma,\end{aligned} \quad (5)$$

where γ is the quadrupole triaxial deformation parameter. So in a system with a non-axially symmetric deformation, the surface radius is written for the quadrupole case as

$$\begin{aligned}R(\theta,\varphi) &= R_0\left\{1+a_{20}Y_{20}+a_{22}\frac{Y_{22}+Y_{22}^*}{\sqrt{2}}\right\},\\ a_{20} &= \beta_2\cos\gamma, \qquad a_{22}=\beta_2\sin\gamma.\end{aligned} \quad (6)$$

For a multipolar deformed systems like nuclei, the central potential is

$$V_{\mathrm{cent}}(r)=V_0f(r), \quad f(r)=\frac{1}{1+\exp\left(\dfrac{r-R}{a}\right)}, \quad (7)$$

and the deformed potential is taken as

$$V_{\mathrm{def}}(\vec{r})=-V_0k(r)\left[\sum_{l}a_{l0}Y_{l0}+\sum_{l,m>0}(a_{lm}Y_{lm}^++b_{lm}Y_{lm}^-)\right], \quad (8)$$

where

$$k(r)=r\frac{\mathrm{d}f(r)}{\mathrm{d}r}.$$

The Hamiltonian of this system can be written as

$$H=T+V=T+V_{\mathrm{cent}}+V_{\mathrm{def}}+V_{\mathrm{sl}}. \quad (9)$$

In the deformed coordinate framework, the Hamiltonian is written as

$$\begin{aligned}H&=\frac{p_r^2}{2M}+\frac{\overrightarrow{l^2}}{2Mr^2}+V_{\mathrm{cent}}+V_{\mathrm{def}}+V_{\mathrm{sl}}\\ &=-\frac{\hbar^2}{2M}\left(\frac{\mathrm{d}^2}{\mathrm{d}r^2}+\frac{2}{r}\frac{\mathrm{d}}{\mathrm{d}r}\right)+\frac{\overrightarrow{l^2}}{2Mr^2}\\ &\quad+V_{\mathrm{cent}}+V_{\mathrm{def}}+V_{\mathrm{sl}},\end{aligned} \quad (10)$$

where the spin-orbit coupling potential takes the form $V_{\mathrm{sl}}=-\frac{1}{2}vV_0g(r)(\overrightarrow{s}\cdot\overrightarrow{l})$ from Ref. [13]. Here the expression for $g(r)$ is $g(r)=\frac{\Lambda^2}{r}\frac{\mathrm{d}f(r)}{\mathrm{d}r}$, where Λ is the reduced Compton wavelength of the nucleon and the parameters are fixed at $v=32$ and $V_0=-51+33\frac{N-Z}{A}$ [14, 15].

The Hamiltonian has been widely used to study the single particle resonant states in deformed nuclei by the coupling-channel method [15]. The Hamiltonian H and wave function ψ are transformed as

$$H_\theta = U(\theta)HU(\theta)^{-1}, \quad (11)$$

$$\psi_\theta = U(\theta)\psi. \quad (12)$$

Here $U(\theta)$ is a complex rotation operator defined in terms of the transformation $\vec{r}\to\vec{r}e^{i\theta}$, and $H_\theta(\psi_\theta)$ is the complex scaled Hamiltonian (wave function) with the complex rotation angle θ. The corresponding complex scaled equation becomes

$$H_\theta\psi_\theta=E_\theta\psi_\theta. \quad (13)$$

We can obtain the bound states, resonant states and non-resonance continuum from Eq. (13). In terms of independence of the calculated results for θ, the resonant states can be picked out. The details can be seen in Ref. [16]. Like axially symmetric nuclei, we combine the CSM (complex scaling method) and Green's function method by defining the complex-scaled Green's function as

$$G^\theta(E)=U(\theta)G(E)U(\theta)^{-1}=\frac{1}{E-H_\theta}. \quad (14)$$

In the coordinate representation, one obtains

$$G^\theta(E,\vec{r},\vec{r'})=\left\langle\vec{r}\right|\frac{1}{E-H_\theta}\left|\vec{r'}\right\rangle. \quad (15)$$

In order to find resonances in the complex scaled Green's function (15), we introduced an extended completeness relation in Ref. [17]:

$$\sum_{b}^{N_b}|\psi_b^\theta\rangle\langle\tilde{\psi}_b^\theta|+\sum_{r}^{N_r}|\psi_r^\theta\rangle\langle\tilde{\psi}_r^\theta|+\int\mathrm{d}E_c^\theta|\psi_c^\theta\rangle\langle\tilde{\psi}_c^\theta|=1, \quad (16)$$

where ψ_b^θ and ψ_r^θ are the complex scaled wave functions for the bound and resonant states, respectively, while ψ_c^θ is the wave function of the rotated continuum. The bra states with tilde represent the bi-orthogonal counterparts of the ket states. Detailed explanations can be found in Ref. [18].

By using the extended completeness relation (16), the level density of the complex scaled Hamiltonian H_θ with the basis number N is expressed as

$$
\begin{aligned}
\rho_\theta(E) &= -\frac{1}{\pi}\mathrm{Im}\int \mathrm{d}\vec{r}\left\langle \vec{r}\left|\frac{1}{E-H_\theta}\right|\vec{r}\right\rangle \\
&= -\frac{1}{\pi}\mathrm{Im}\int \mathrm{d}\vec{r}\left[\sum_b^{N_b}\frac{\psi_b^\theta(\vec{r})\tilde{\psi}_b^{\theta*}(\vec{r})}{E-E_b}\right. \\
&\quad \left. +\sum_r^{N_r}\frac{\psi_r^\theta(\vec{r})\tilde{\psi}_r^{\theta*}(\vec{r})}{E-E_r^\theta}+\int \mathrm{d}E_c^\theta\frac{\psi_c^\theta(\vec{r})\tilde{\psi}_c^{\theta*}(\vec{r})}{E-E_c^\theta}\right], \quad (17)
\end{aligned}
$$

where E_b, E_r^θ and E_c^θ represent respectively the energy eigenvalues of H_θ for the bound states, resonant states and rotated continuum. N_b and N_r are the numbers of bound states and resonant states, respectively. Due to the normalization of the wave functions, the integration $\vec{r}$ for the bound and resonant states in Eq. (17) is unity. For the continuum, however, there appears a singularity in the integration $\vec{r}$, which can be eliminated by using the basis expansion method in the discretization of the energy spectrum. Then, the approximate density of states can be expressed as

$$
\begin{aligned}
\rho_\theta^N(E) &= \sum_b^{N_b}\delta(E-E_B)+\frac{1}{\pi}\sum_r^{N_r}\frac{\Gamma_r/2}{(E-E_r)^2+\Gamma_r^2/4} \\
&\quad +\frac{1}{\pi}\sum_c^{N-N_b-N_r}\frac{\varepsilon_c^I}{(E-\varepsilon_c^R)^2+\varepsilon_c^{I2}}, \quad (18)
\end{aligned}
$$

where the bound state energies $E_b(b = 1,2,...,N_b)$, the resonance complex energies $E_r^\theta = E_r-\mathrm{i}\Gamma_r/2(r = 1,2,...,N_r)$, and the rotated continuum energies $\varepsilon_c^\theta = \varepsilon_c^R-\mathrm{i}\varepsilon_c^I(c=1,2,...,N-N_b-N_r)$.

As there are approximations in realistic calculations, $\rho_\theta^N(E)$ depends slightly on θ. The dependence can be removed by subtracting the background of H_θ, which is defined as the density of continuum states $\rho_\theta^{0N}(E)$:

$$
\rho_\theta^{0N}(E)=\frac{1}{\pi}\sum_k^N\frac{\varepsilon_k^{0I}}{(E-\varepsilon_k^{0R})^2+\varepsilon_k^{0I2}}, \quad (19)
$$

where $\varepsilon_k^0(\theta)=\varepsilon_k^{0R}-\mathrm{i}\varepsilon_k^{0I}$ are the eigenvalues of the asymptotic Hamiltonian H_θ^0 in the form of H_θ with $r \to \infty$. After subtracting the background of H_θ, we obtain the continuum level density $\Delta\rho(E)$ as the difference between the density of states $\rho_\theta^N(E)$ and the density of continuum states $\rho_\theta^{0N}(E)$:

$$
\Delta\rho(E)=\rho_\theta^N(E)-\rho_\theta^{0N}(E). \quad (20)
$$

Because the background of H_θ has been removed, the continuum level density $\Delta\rho(E)$ is almost independent of θ. Hence, it is more appropriate to explore resonances by using the continuum level density $\Delta\rho(E)$ in the CGF calculations. For the other systems in Ref. [13], Ω is the projection of the total angular momentum in the axial symmetry. It is no longer a good quantum number in the present calculation, but the parity is still a good quantum number, so we can diagonalize the Hamiltonian in the subspace with the same parity.

3   Results and discussion

With the formalism in the previous section, we explore the resonant states in triaxially deformed nuclei. In our calculations, the complex scaled Eq. (13) is solved by expansion in the HO basis with 60 oscillator shells, which is characterized by the parameter $b_0=1.8927$ fm. The b_0 value belongs to the plateau in Ref. [19, 20], where the resonance energy hardly varies with b_0 on the plateau. Since there is still no observable β value for ^{43}S from experiment, the theoretical value of $\beta=0.196$ is used for the moment, which is taken from the finite range droplet model-2012 (FRDM2012) [21]. For convenience of calculation, $\beta = 0.2$ is used in our calculation. The parameters of the potential remain the same as those for nucleus ^{43}S, except the depth of the potential $V_0=-42.70$ MeV, which is reduced by about 0.14 MeV from its standard value. This small reduction is made to reproduce the neutron separation energy of ^{43}S. For example, the diffuseness is fixed at $a=0.67$ fm, $r_0=1.27$ fm, and the radius $R=r_0A^{1/3}$, where A is a nuclear mass number. Then we obtain the S_n value 2.66 MeV, which is appropriate for the calculation in the paper and close to 2.63 MeV, which is the S_n value of ^{43}S in Ref. [22].

An illustrated example for the continuum level density $\Delta\rho(E)$ with negative parity is plotted in Fig. 1. Based on the details in Ref. [23], we can determine the resonance parameters like energy and width. The sharp peak emerging in $\Delta\rho(E)$ represents a resonant state. The energy of the resonant state can be expressed by the position of the peak at the transverse axis. The distance between these two crossings corresponds to the width of the resonant state. These two crossings occur at a horizontal line at half the height of the peak. One crossing corresponds to $E_r-\Gamma/2$ and the other to $E_r+\Gamma/2$. From Ref. [12], the complex angle $\theta = 14.5°$ is the optimal value. To further make the parameter appropriate, we list the resonant energy with the change of θ from $\theta=10.5°$ to $15.5°$. We find the difference is very small, as shown in Table 1. So $\theta=14.5°$ is adopted in the following CGF calculations. In Fig. 1, the three peaks correspond to three resonance states, which is different from the quadrupole axial deformation with only one peak. The breaking of axial symmetry is the reason why the continuum level

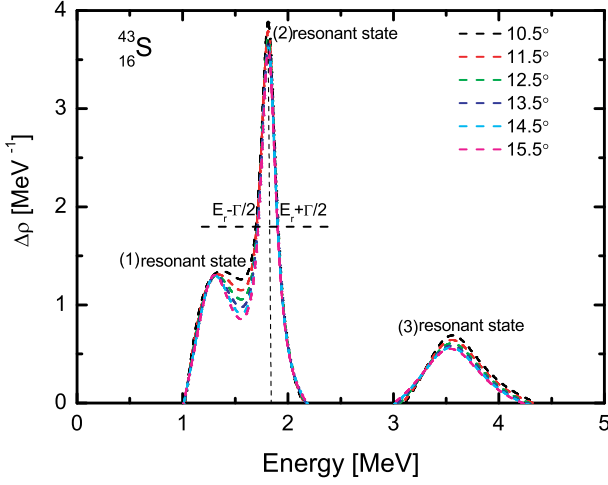density $\Delta\rho(E)$ has more than one peak.

Fig. 1. (color online) Variation of the eigenvalues of $\Delta\rho(E)$ with θ for negative parity states, where the complex scaling parameter θ varies from $10.5°$ to $14.5°$ in steps of $1°$, $\beta = 0.2$, and the triaxial deformation $\gamma = 30°$.

Table 1. Changes in the energy of resonant states for the negative parity states with the complex angle θ by the CGF method. The parameters are the same as Fig.1.

θ	E_r/MeV	E_r/MeV	E_r/MeV
$10.5°$	1.3735	1.8109	3.5591
$11.5°$	1.3397	1.8118	3.5557
$12.5°$	1.3234	1.8125	3.5520
$13.5°$	1.3149	1.8132	3.5483
$14.5°$	1.3097	1.8135	3.5446
$15.5°$	1.3052	1.8128	3.5405

To further analyze the influence of the triaxial deformation parameters γ on the resonances, the resonant states are shown with positive parity in Fig. 2. and Fig. 3. In the CGF calculations, the resonance parameters are determined by the position and height of the resonant peaks. With $\gamma = 0°$, it comes back to an axially symmetric quadrupole-deformed nucleus. There are five resonant peaks corresponding to the degenerate $1g_{9/2}$ in Fig. 2. As the triaxial deformation is increased, more considerable variations can be seen in Fig. 3. One can see that the resonances (with energy shown in green) disappear as we proceed from $\gamma = 15°$ to $\gamma = 60°$. This demonstrates that the triaxial deformation obviously affects the creation or disappearance of resonant states.

For comparison, Fig. 4 shows the results from the CSM calculations. In the CSM calculations, the resonance parameters are determined by using the θ trajectory. As one can see, it is difficult to identify which ones are the resonances, but we also find the resonances close

to the Fermi surface. The CSM seems to be less able to achieve level structures. In contrast, we can obtain the resonance numbers and energy by the continuum level density $\Delta\rho(E)$ conveniently and accurately, especially for resonances close to the Fermi surface. For example, the resonance energy at $\gamma = 15°$ is 1.3657 MeV, which impacts the level structure. In order to further illustrate our results, we list the energy in several different triaxial deformations in Table 2. It shows the CGF succeeds in identifying them but the CSM fails. We see that it displays the resonance states clearly, and the lower energy resonance states can be calculated. So the values determined from the resonant peak using this method should be more reliable.
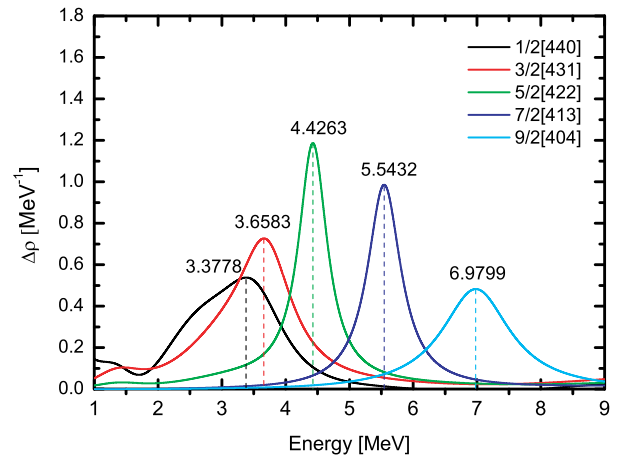

Fig. 2. (color online) Variation of the continuum level density $\Delta\rho(E)$ with $\gamma = 0°$ for the states $1g_{9/2}$. And the $\theta = 14.5°$ $\beta = 0.2$.

Table 2. Changes in the energy of resonant states for the positive parity states with the γ values by the CGF method. And the $\theta = 14.5°$ $\beta = 0.3$.

γ	E_r/MeV	γ	E_r/MeV
$5°$	1.1483	$10°$	1.1711
$15°$	1.2077	$20°$	1.2559
$25°$	1.3114	$30°$	1.3668
$35°$	1.4091	$40°$	1.4233
$45°$	1.4117	$50°$	1.3925
$55°$	1.3714	$60°$	1.3572

In order to further understand of the origin of the triaxiality, we show the single-particle levels in Fig. 5. In the left- and right-hand panels, we show single-particle levels with $\gamma = 0°$ and $\gamma = 60°$, respectively. In the middle panel, the neutron levels are plotted as functions of deformation γ for a fixed value of $\beta = 0.3$. The $2p_{3/2}$ and $1f_{7/2}$ levels degenerate at $\beta = 0.18$ in the left-hand panel of Fig. 5, so the $2p_{3/2}$ level determines the single neutron separation energy S_n at $\beta = 0.2$. In this way, the levels
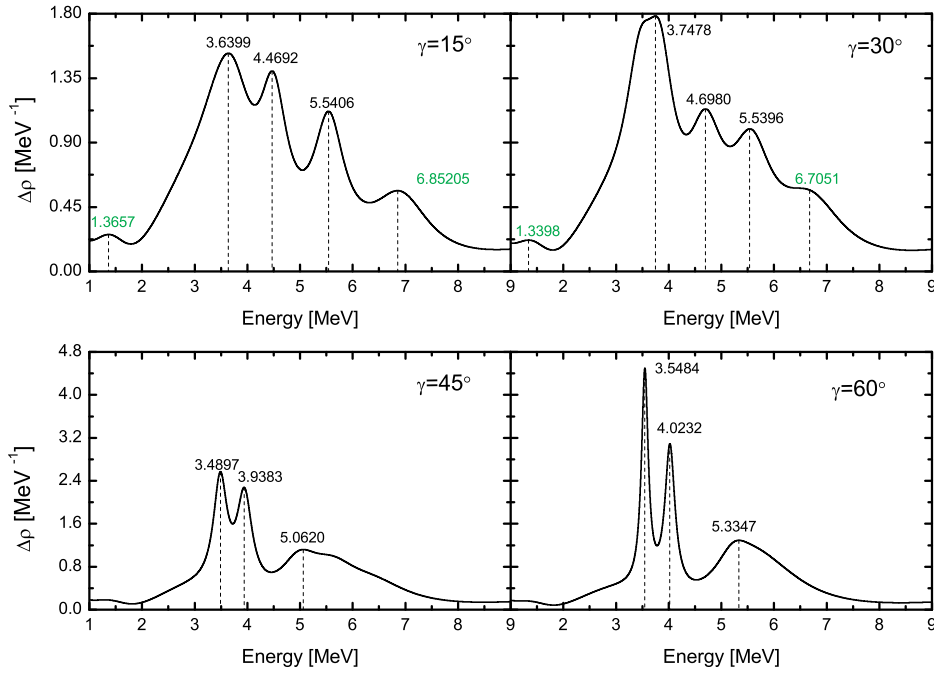
Fig. 3.   (color online) Variation of the energy of resonant states for the positive parity states with the triaxial deformation γ by the CGF method. Other parameters are the same as Fig. 2.
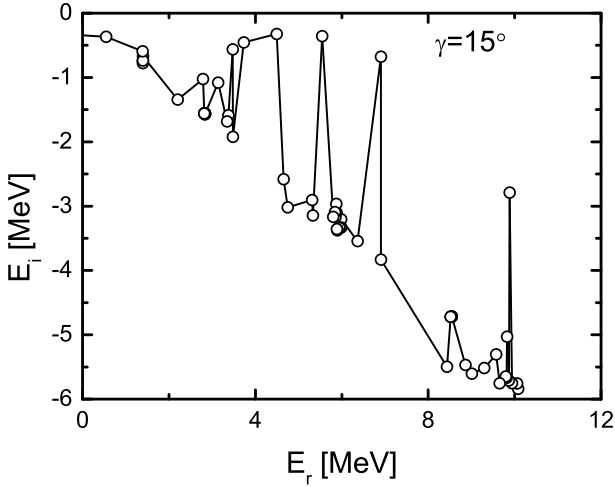

Fig. 4.   Resonant states calculated using the results obtained with the CSM. $\theta = 14.5°$ $\beta = 0.2$, and the triaxial deformation $\gamma = 15°$.

have experienced the process of the spherical configuration; we follow the single-nucleon levels, then for this fixed value of β the path goes from $\gamma = 0°$ to $\gamma = 60°$ (middle panel) and finally, back to $\gamma = 60°$. This level structure is similar to the Nilsson diagram of single particle states in Ref. [24]. The traditional magic numbers $N = 40$, $N = 20$, and the new magic number $N = 14$, appear in this region. The $N = 40$, $N = 20$, $N = 14$ shell gaps vary and even vanish depending on β and γ. The three shell gaps have gap energies of 2.9 MeV, 5.0 MeV, and 3.4 MeV respectively at a spherical shape. At large pro-

late deformation ($\beta > 0.3$), the shell gaps are completely lost. In the triaxially deformed region, the $1f_{7/2}$ and $2p_{3/2}$ levels which originate in the spherical region are reversed for $\beta = 0.3$ and $\gamma = 35°$. The $N = 28$ shell gap also emerges with approximately 2.5 MeV at spherical shape, then gradually quenches in the deformed case. From Fig. 5, the change of resonances can be clearly observed. All of these intuitively show that the influence of triaxial deformation on the energy level structure is indispensable.

Considering that the width is an important physical quantity for the resonant states, it is meaningful to study the influence of the triaxial deformation on the width. Because γ values deeply affect the number of resonances, we cannot get continuously changing width. However, we can illustrate the influence by the following examples. From the fourth line from the top in the middle panel in Fig. 5, the width of the positive parity is 1.7588 MeV with $\gamma = 30°$. For the triaxial deformation with $\gamma = 0°$ to $60°$, the deformation is maximum with $\gamma = 30°$. In Ref. [12], it is known that such a broad state is extremely unstable. But when the γ values become 35°, 55°, 60°, the widths are 1.5073 MeV, 0.2268 MeV, and 0.1247 MeV respectively. A rapid change happens in width with increasing γ. The γ deformation plays a very important role in state evolution. Because the width is a reciprocal of lifetime [25, 26], it means the lifetime of the resonant states become longer and longer with increasing γ. This will be helpful to explore exotic level structures.
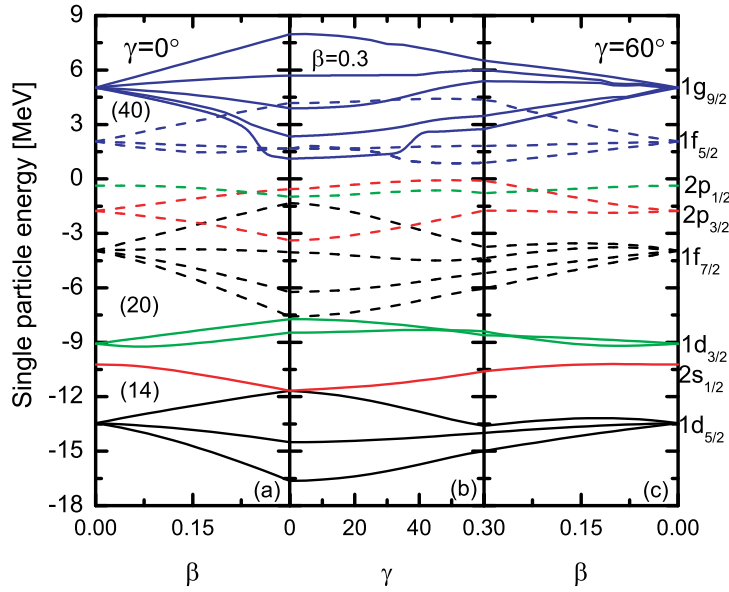
Fig. 5.   (color online) Calculated single-particle levels with deformation as functions of the quadrupole deformation parameters β and γ.
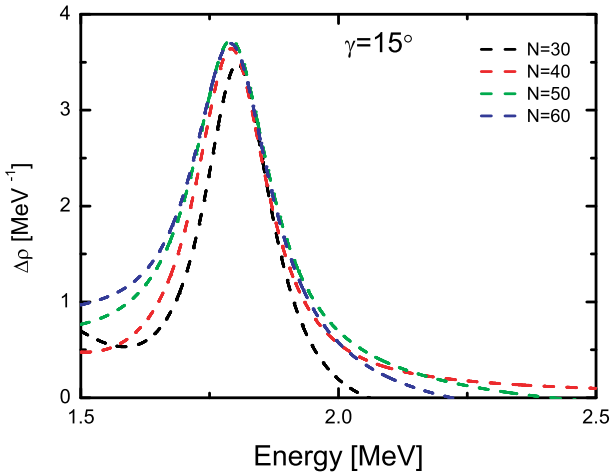

Fig. 6.   (color online) Variation of continuum level density $\Delta\rho(E)$ with different main shell numbers of the harmonic oscillator basis $N = 30, 40$, and $50, 60$ for one resonance of negative parity states, with complex rotation angle $\theta = 14.5°$, $\gamma = 15°$, and $\beta = 0.2$.

Although the CGF method is particularly suitable to determine the resonance parameters with the triaxial deformation, we still need to check the dependence of the calculation on the basis size, because the presented results are achieved by basis expansion with a finite number. In Fig. 6, we display the variation of the continuum level density $\Delta\rho(E)$ with the size of the basis for one resonance of negative states with $\gamma = 15°$. For comparison, we select the main shell numbers of the harmonic oscillator basis $N = 30, 40, 50, 60$. When $N = 50, 60$, $\Delta\rho(E)$ are almost coincident. This indicates that the positions

of the peaks corresponding to the energy of the resonant states almost completely coincide. Actually, the continuum level density $\Delta\rho(E)$ is independent of N as long as the size of basis is large enough. So we choose $N = 60$ to study the resonant states. This is also convenient and compared to the quadrupole deformation.

4   Summary

In summary, we have used the complex scaled Green's function method to describe resonances characterized by the quadrupole triaxial deformation parameter γ besides the axial deformation parameter β. A theoretical formalism has been presented in detail. Resonant states have been explored by calculating the continuum level density $\Delta\rho(E)$ for ^{43}S. We have explained why the continuum level density is different from the axial symmetrical system. We have checked the dependence of the continuum level density on the complex scaling parameter θ and the size of the basis, obtaining convergent results. In addition, we have investigated the influence of deformations on the resonances. With the γ deformation, the positions and the numbers of resonance peaks both change. We have also calculated the single-particle levels, which show the effect of triaxial deformation on energy levels. The reversal of energy level and the appearance of magic numbers are affected by the quadrupole triaxial deformation parameter γ, which is helpful to recognize shell structure and its evolution in deformed nuclei. Especially, the width of the resonant states shows lifetime evolution with deformation and is helpful to recognize shell structure in exotic nuclei.

References

1 N. Tajima and N. Suzuki, Phys. Rev. C, **64**: 037301 (2001)
2 P. Ring and P. Schuck, The Nuclear Many-Body Problem (Springer-Verlag, Berlin, 1980)
3 P. Möller, R. Bengtsson, B. G. Carlsson, P. Olivius, and T. Ichikawa, Phys. Rev. Lett., **97**: 162502 (2006)
4 Y. Fu, H. Mei, J. Xiang, Z. P. Li, J. M. Yao, and J. Meng, Phys. Rev. C, **87**: 054305, (2013)
5 M. Kimura, Y. Taniguchi, Y. Kanada-En'yo, H. Horiuchi, and K. Ikeda, Phys. Rev. C, **87**: 011301(R) (2013)
6 J. Xiang, J. M. Yao, Y. Fu, Z. H. Wang, Z. P. Li, and W. H. Long, Phys. Rev. C, **93**: 054324 (2016)
7 A. Bohr and B. R.Mottelson, Nuclear Structure (Benjamin, NewYork, 1975), Vol. II.
8 S. Frauendorf and J. Meng, Nucl. Phys. A, **617**: 131 (1997)
9 J. Meng, J. Peng, S. Q. Zhang, and S.-G. Zhou, Phys. Rev. C, **73**: 037303 (2006)
10 J.-P. Delaroche, M. Girod, J. Libert, H. Goutte, S. Hilaire, S. Péru, N. Pillet, and G. F. Bertsch, Phys. Rev. C, **81**: 014303 (2010)
11 S. F. Shen, S. J. Zheng, F. R. Xu, and R. Wyss, Phys. Rev. C, **84**: 044315 (2011)
12 X. X. Shi, M. Shi, Z. M. Niu, T. H. Heng, J. Y. Guo, Phys. Rev. C, **94**: 024302 (2016)
13 Q. Liu, J. Y. Guo, Z. M. Niu, and S. W. Chen, Phys. Rev. C, **86**: 054312 (2012)
14 I. Hamamoto, Phys. Rev. C, **85**: 064329 (2012)
15 I. Hamamoto, Phys. Rev. C, **72**: 024301 (2005)
16 M. Shi, J. Y. Guo, Q. Liu, Z. M. Niu, and T. H. Heng, Phys. Rev. C, **92**: 054313 (2015)
17 T. Myo, A. Ohnishi, and K. Katō, Prog. Theor. Phys., **99**: 801 (1998)
18 T. Berggren, Nucl. Phys. A, **109**: 265 (1968)
19 J. Y. Guo, M. Yu, J. Wang, B. M. Yao, and P. Jiao, Comput. Phys. Commun., **181**: 550 (2010)
20 J. Y. Guo, J. Wang, B. M. Yao, and P. Jiao, Int. J. Mod. Phys. E, **19**: 1357 (2010)
21 P. Möller, A. J. Sierk, T. Ichikawa, and H. Sagawa, At. Data Nucl. Data Tables, **109-110**: 1 (2016)
22 National Nuclear Data Center, http://www.nndc.bnl.gov
23 M. Shi, X. X. Shi, Z. M. Niu, T. T. Sun and J. Y. Guo, Eur. Phys. J. A, **53**: 40 (2017)
24 I. Ragnarsson and S. G. Nilsson, Phys. Rep., **45**: 1 (1978)
25 J. Aguilar and J. M. Combes, Commun. Math. Phys., **22**: 269 (1971); E. Balslev and J. M. Combes, ibid., **22**: 280 (1971)
26 R. Suzuki, T. Myo, and K. Katō, Prog. Theor. Phys., **113**: 1273 (2005)